Numerical and experimental study of the heat transfer process in friction stir welding

M Song and **R Kovacevic***
Research Center of Advanced Manufacturing, Department of Mechanical Engineering,
Southern Methodist University, Richardson, Texas, USA

Abstract: A mathematical model to describe the detailed three-dimensional transient heat transfer process in friction stir welding (FSW) is presented. This work is both theoretical and experimental. An explicit central differential scheme is used in solving the control equations, the heat transfer phenomena during the tool penetrating, the welding and the tool-removing periods that are studied dynamically. The heat input from the tool shoulder is modelled as a frictional heat and the heat from the tool pin is modelled as a uniform volumetric heat generated by the plastic deformation near the pin. The temperature variation during the welding is also measured to validate the calculated results. The calculated results are in good agreement with the experimental data.

Keywords: friction stir welding, heat transfer, modelling, welding, aluminium alloy

NOTATION

c	heat capacity (J/kg K)
F_f	surface friction force (N)
F_n	normal force (N)
F_p	translation force (N)
h	thickness of the workpiece (m)
h_c	coefficient of heat convection (W/m^2 K)
H	enthalpy (J/Kg)
k_x, k_y, k_z	thermal conductivities (W/m K)
$\boldsymbol{n}$	normal vector of boundary Γ
q	heat flux (W/m^2)
r_p	radius of the pin (m)
r_{sh}	radius of the shoulder (m)
S	heat source term (W/m^3)
t	time (s)
T	temperature (K)
v_i	slip velocity (m/s)
v_w	weld speed (m/s)
x, y, z	space coordinate (m)
$\bar{Y}$	average yield stress (Mpa)
λ	helix angle of the pin thread
μ	coefficient of friction

The MS was received on 12 June 2002 and was accepted after revision for publication on 6 September 2002.
**Corresponding author: Research Center of Advanced Manufacturing, Department of Mechanical Engineering, Southern Methodist University, 1500 International Parkway, Suite 100, Richardson, TX 75081, USA.*

1 INTRODUCTION

Friction stir welding (FSW) is a relatively new solid-state joining process, developed at the Welding Institute (TWI), England, in 1991 [**1**]. This new technology has proven to be very successful in joining aluminium alloys. It can produce superior mechanical properties when compared to the typical electrical arc welding process and therefore has gained considerable interest in the past decade [**2**, **3**].

Figure 1 illustrates the schematic diagram of FSW as applied to a butt joint of two flat plates. The workpiece to be welded is supported by a backing plate and clamped rigidly by an anvil to prevent lateral movement during the welding. A cylindrical tool with a pin rotates and slowly plunges into the workpiece along the joint line until the tool shoulder contacts the workpiece top surface. The rotation of the tool generates surface friction heat and plasticizes a cylindrical column of metal around the pin.

To improve understanding of this new welding technique, a detailed investigation of the process is required. Modelling can play a key role in the FSW research by accelerating the development and reducing the experimental costs.

A detailed model of heat generation and conduction for FSW is useful:

1. A heat transfer model is helpful in predicting the temperature pattern during the welding.

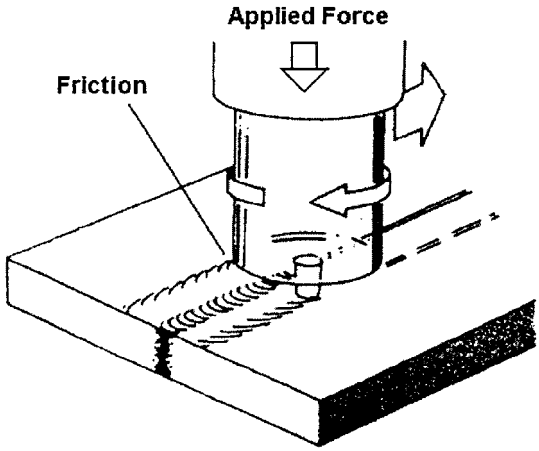

Fig. 1 Schematic diagram of FSW

2. A predicted temperature field can be used in evaluating the heat affected zone (HAZ) microstructure and hardness of the weld.
3. A provided temperature field is necessary in determining the temperature-dependent viscosity for material flow modelling.

It is well known that welding relies on heat generation during the process to join the workpiece together. As for FSW, it is generally considered that there are two main heat sources:

(a) the friction heat generated at the interface between the tool shoulder and the workpiece and
(b) the material plastic deformation heat that generated near the tool pin. The friction heat input from the tool shoulder is believed to be the main heat input in the FSW process [**4**–**6**].

In recent years, significant progress has been made in the modelling heat transfer process during FSW [**4**–**15**]; thermal couple measured temperature distribution during the welding has also been attained [**16**–**18**].

In 1998, Chao and Qi published a three-dimensional heat transfer model for FSW [**4**]. In their paper, the heat flux input from the tool shoulder is assumed to be constant, and the value is determined by a trial-and-error procedure until the calculated temperatures match with all the measured ones. The finite element method (FEM) is used in their modelling. Frigaard *et al.* [**5**, **6**] calculated the heat input from the workpiece/tool shoulder surface as the slide friction heat generated by a rotating circular shaft to a plate surface under an axial load. The finite difference method is used in the numerical solution. In the calculations of Frigaard *et al.*, the coefficient of friction during the welding is adjustable in order to ensure that the calculated temperatures at all points do not exceed the material melting point. The Rosenthal equation for modelling the heat transfer of a thin plate is also used in modelling the heat transfer for FSW [**7**, **8**]. In Russell and Shercliff's work [**8**], the heat generation in the tool shoulder/workpiece interface is calculated by the Midling sticking friction solution of convectional friction welding, which could better describe the friction mechanism in FSW.

In these models, the heat generated from the pin as well as the heat generated by the plastic deformation at the tool/shoulder interface are not included. Colegrove published a three-dimensional heat transfer model and gave an expression for calculating the heat generated by the pin during FSW [**9**]. It is concluded in his paper that the heat generated from the pin should not be neglected. Bendzsak *et al.* [**10**] and Smith *et al.* [**11**] applied the computational fluid dynamics (CFD) method in modelling the heat and material flow process during FSW, where the material is assumed to be a kind of non-Newtonian fluid in their modelling, This application is a good attempt at coupling the heat transfer modelling and material flow modelling in FSW.

The heat transfer process during tool penetration and extraction is not currently modelled in detail in the presented models. Such detailed heat transfer modelling will be important if preheat is introduced in FSW [**19**].

In this paper, a detailed transient heat transfer model for FSW is presented and applied in analysing the heat transfer process of an aluminium alloy during FSW. In this model, the heat transfer process during tool penetration and pulling out are studied, and the heat generated by the tool pin is also considered. The explicit central differential scheme is used in the numerical solutions. A FORTRAN program code is developed to solve the control equations numerically.

2 MODEL DESCRIPTIONS

In order to simplify the mathematical model, the FSW process is divided into the following three periods:

1. *The penetrating period*: from the instant when the tool pin contacts the workpiece surface until the tool shoulder contacts the workpiece surface.
2. *The welding period*: from the instance when the tool–shoulder contacts the workpiece until the tool stops traversing. This period is the main period of the welding.
3. *The pulling-up period*: from the instance when the tool starts pulling out until the pin completely leaves the workpiece.

The following assumptions are introduced to simplify the model:

1. All the frictional energy is converted to heat and exerted on the workpiece.
2. The material deformation at the workpiece top surface during the weld is negligible.
3. The frictional heat from the tool pin during the welding is negligible.
4. The tool pin is in the shape of a cylinder.

2.1 Control equation

The governing equation describing the heat transfer process in the workpiece can be written as:

$$\frac{\partial H(T)}{\partial t} = \frac{\partial}{\partial x}\left[k_x(T)\frac{\partial T}{\partial x}\right] + \frac{\partial}{\partial y}\left[k_y(T)\frac{\partial T}{\partial y}\right] + \frac{\partial}{\partial z}\left[k_z(T)\frac{\partial T}{\partial z}\right] + S \quad (1)$$

and

$$H(T) = \int_0^T c_p(T)\rho(T)\,\mathrm{d}T \quad (2)$$

where H is enthalpy, c is the material heat capacity, ρ is the material heat density, k is the material heat conductivity and S is the heat generation source term.

2.2 Heat generation

2.2.1 *Heat generated by the tool shoulder*

According to the assumptions, the heat input from the tool shoulder can be calculated from the frictional heat generation at the workpiece/tool shoulder interface during the welding. The plastic deformation heat generated at the tool shoulder/workpiece interface is neglected.

As shown in Fig. 2, the local friction force at every calculated point can be calculated from

$$F_{\mathrm{f}_i} = \mu F_{\mathrm{n}_i} \quad (3)$$

where F_{f_i} is the local friction force at each grid mesh point and F_{n_i} is the normal force applied to the workpiece. Therefore the local heat generation rate can be calculated as

$$q_i = F_{\mathrm{f}_i} v_i \quad (4)$$

where q_i is a local heat generation rate and v_i is the relative slip velocity. Because $v_i = R_i\omega$ and $\omega = 2\pi n$, therefore

$$q_i = 2\pi\mu F_{\mathrm{n}_i} R_i N \quad (5)$$

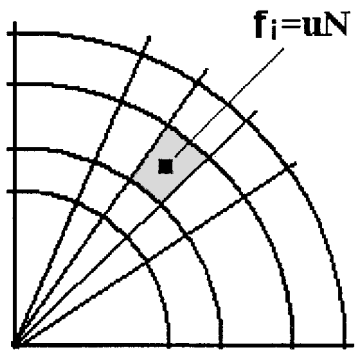

Fig. 2 Local heat input from the shoulder

where N is the rotational speed and R_i is the distance of the calculated point from the tool axis.

2.2.2 *Heat generated by the tool pin*

In this model, the material plastic deformation heat generated by the tool pin is assumed to be the only heat generated by the tool pin during the welding. This heat is simplified to a uniform volumetric heat generation within a cylinder volume. This volumetric heat generation is summarized as the source term in equation (1).

The diameter of the cylinder representing the plastically deformed material is larger than the diameter of the tool pin; it depends on the rotational speed and the pin-thread pattern. However, due to lack of accurate data, this diameter is assumed to be equal to the pin diameter in this paper.

The heat generated by the plastic deformation consists of three parts: (a) heat generated by shearing of the material; (b) heat generated by friction on the threaded surface of the pin; and (c) heat generated by friction on the vertical surface of the pin. The total heat generation from the pin can be calculated from [**9**]

$$Q_{\mathrm{pin}} = 2\pi r_{\mathrm{p}} h \bar{Y}\frac{V_{\mathrm{m}}}{\sqrt{3}} + \frac{2\mu\bar{Y}\pi r_{\mathrm{p}} h V_{\mathrm{rp}}}{\sqrt{3(1+\mu^2)}} + \frac{4F_{\mathrm{p}}\mu V_{\mathrm{m}}\cos\theta}{\pi} \quad (6)$$

where

$$\theta = 90^\circ - \lambda - \tan^{-1}(\mu)$$

$$V_{\mathrm{m}} = \frac{\sin\lambda}{\sin(180^\circ - \theta - \lambda)} v_{\mathrm{p}}$$

$$V_{\mathrm{rp}} = \frac{\sin\theta}{\sin(180^\circ - \theta - \lambda)} v_p$$

$$v_{\mathrm{p}} = r_{\mathrm{p}}\omega$$

where r_{p} is the radius of the tool pin, h is the thickness of the workpiece, $\bar{Y}$ is the average shear stress of the material, F_{p} is the translation force during the welding and λ is the helix angle of the thread. In this model, the last two terms in equation (6) are neglected because the tool pin thread detail is not considered in the model.

2.3 Boundary conditions and initial field

1. Tool shoulder/workpiece boundary. The boundary condition at the tool shoulder/workpiece interface is a Neumann condition and can be calculated from the frictional heat:

$$k\left.\frac{\partial T}{\partial n}\right|_{\Gamma} = q_i \quad (7)$$

2. The convection boundary conditions. The boundary conditions of the workpiece surfaces exposed to the air are Neumann conditions. The boundary in contact with the back-up plate can be simplified as a Neumann condition with an effective convection coefficient. The Neumann condition in all the convection boundaries can be expressed as

$$k \left.\frac{\partial T}{\partial n}\right|_{\Gamma} = h(T - T_0) \tag{8}$$

where n is the normal direction vector of boundary Γ and h is the convection coefficient.

3. Initial condition. The initial condition in the calculation is

$$T(x, y, z, 0) = T_i \tag{9}$$

3 NUMERICAL SOLUTION

3.1 Numerical scheme

An explicit central difference scheme is used in the discretization of the control equations. The discrete equations for all inner points are (see Fig. 3)

$$\begin{aligned}\rho c \frac{T_{i,j,k}^{(n+1)} - T_{i,j,k}^{(n)}}{\Delta t} &= k_x \frac{T_{i+1,j,k}^{(n)} - 2T_{i,j,k}^{(n)} + T_{i-1,j,k}^{(n)}}{\Delta x^2} \\ &\quad + k_y \frac{T_{i,j+1,k}^{(n)} - 2T_{i,j,k}^{(n)} + T_{i,j-1,k}^{(n)}}{\Delta y^2} \\ &\quad + k_z \frac{T_{i,j,k+1}^{(n)} - 2T_{i,j,k}^{(n)} + T_{i,j,k-1}^{(n)}}{\Delta z^2} + S\end{aligned} \tag{10}$$

The time marching procedures of all inner points are

$$\begin{aligned}T_{i,j,k}^{(n+1)} &= T_{i,j,k}^{(n)} + \frac{1}{\rho c} \\ &\quad \times \left[k_x \frac{T_{i+1,j,k}^{(n)} - 2T_{i,j,k}^{(n)} + T_{i-1,j,k}^{(n)}}{\Delta x^2} \right. \\ &\quad + k_y \frac{T_{i,j+1,k}^{(n)} - 2T_{i,j,k}^{(n)} + T_{i,j-1,k}^{(n)}}{\Delta y^2} \\ &\quad \left. + k_z \frac{T_{i,j,k+1}^{(n)} - 2T_{i,j,k}^{(n)} + T_{i,j,k-1}^{(n)}}{\Delta z^2} + S \right] \Delta t\end{aligned} \tag{11}$$

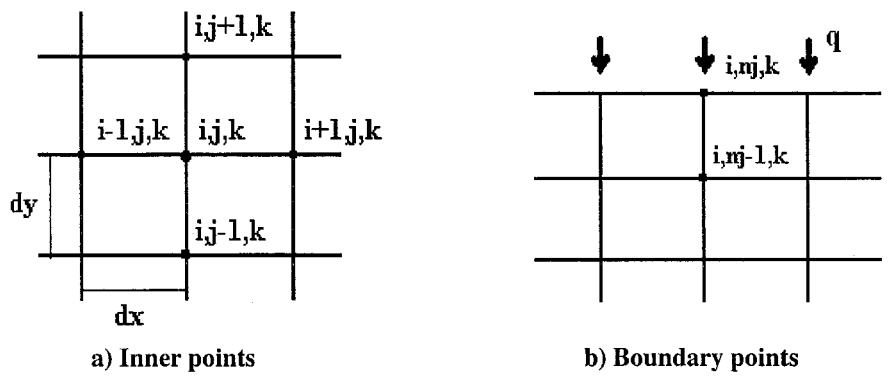

Fig. 3 Finite difference scheme

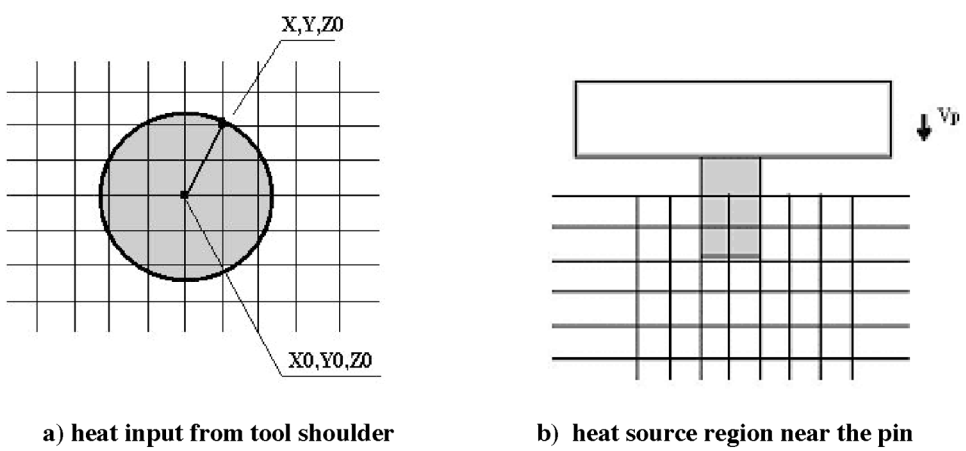

Fig. 4 Boundary restriction

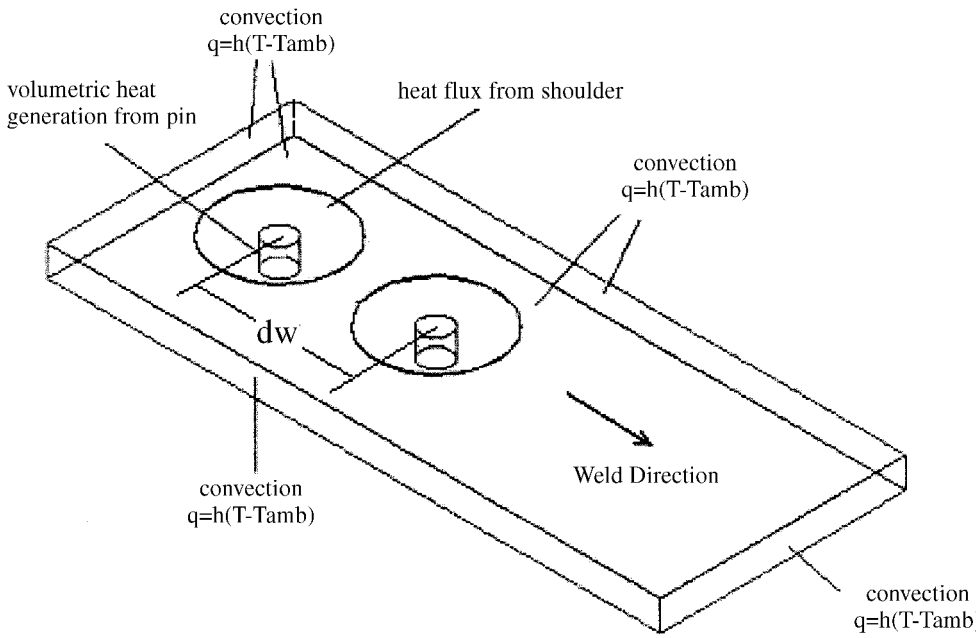

Fig. 5 Boundary moving along the weld direction

where $T_{i,j,k}^{(n)}$ and $T_{i,j,k}^{(n+1)}$ are the temperatures at point (i, j, k) at time n and $n+1$ respectively and Δt is the time step in the calculation. If the calculated temperature reaches the material melting temperature, the heat input from the tool is adjusted to zero.

3.2 Boundary discretization

The discretization of the heat flux condition at the tool shoulder/workpiece contact surface is

$$T_{i,nj,k}^{(n)} = T_{i,nj-1,k}^{(n)} + q_{\mathrm{f}} \frac{\Delta x}{k} \tag{12}$$

The discretization of the convection condition in other areas on the workpiece upper surface is

$$T_{i,nj,k}^{(n)} = \frac{k_y T_{i,nj-1,k}^{(n)} + h\,\Delta y T_0}{k_y + h\,\Delta y} \tag{13}$$

Similar boundary discretizations are applied to all other convection boundaries.

3.3 Boundary restriction

The heat flux input condition is applied only to the points within the tool shoulder covered surface ($j = nj$), while the convection boundary condition is applied to all other points in the upper surface. The heat flux input condition is restricted to a moving circle. The distance of all points within this circle from the tool axis is smaller than the tool shoulder radius r_{sh} (see Fig. 4):

$$\mathrm{dist}_1 = \sqrt{(x_{i,j,nk} - x_{i0,j0,nk})^2 + (y_{i,j,nk} - y_{i0,j0,nk})^2} \leqslant r_{\mathrm{sh}}$$
$$(i = 2, 3, \ldots, ni-1,\ j = 2, 3, \ldots, nj-1) \tag{14}$$

The heat generated by the plastic deformation moves at the welding speed in the form of a moving cylinder during the welding. The distance of all points in this cylinder from the tool axis is smaller than the tool pin radius r_{p}:

$$\mathrm{dist}_2 = \sqrt{(x_{i,j,k} - x_{i0,j0,k})^2 + (y_{i,j,k} - y_{i0,j0,k})^2} \leqslant r_{\mathrm{p}}$$
$$(i = 2, 3, \ldots, ni-1,\ j = 2, 3, \ldots, nj-1,\ k = 2, \ldots, nk-1) \tag{15}$$

Both the heat flux input boundary and the volume of the plastic heat generation move at the welding speed along the joint line (see Fig. 5):

$$x_0 = v_{\mathrm{w}} t \tag{16}$$

During the pin plunging in and pulling out periods, the heights of cylinders representing the generated heat are

Table 1 Input parameters for the calculation

Density (kg/m^3)	Heat conductivity (W/m K)	Coefficient of friction	Rotation speed (r/min)	Weld speed (mm/s)	Applied force (kN)
2700	167	0.4	637	1.59	25

calculated from the tool pin penetration speed and the pulling out speed respectively:

$$dz = v_p \, dt \tag{17}$$

$$dz = v_{po} \, dt \tag{18}$$

where v_p and v_{po} are the tool pin penetration speed and tool pulling out speed respectively.

3.4 Material properties

The heat conduction coefficients k_x, k_y and k_z are assumed to be constant and equal during the welding. The material properties of Al 6061/T6 and the welding conditions used in the calculation are listed in Table 1.

4 EXPERIMENTAL RESULTS

For the purpose of validating the calculated results, the FSW experiments have been carried out under controlled conditions. The experimental setup is shown in Fig. 6. The tool rotational speeds are 344, 637 and 914 r/min. The corresponding weld speeds are 1.59 and 3.18 mm/s. The diameter of the tool shoulder is 50 mm and the diameter of the tool pin is 12 mm. Two Al 6061/T6 plates, 254.0 mm in length, 102.0 mm in width and 12.7 mm in thickness are butt welded.

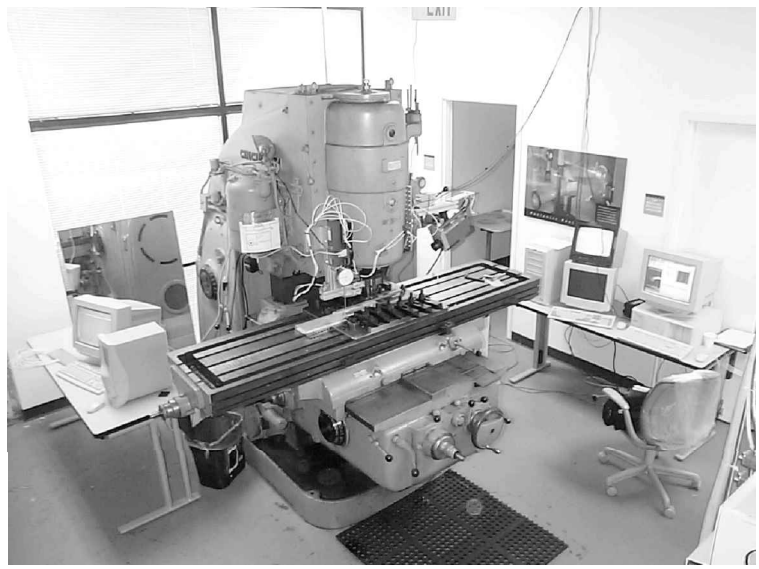

Fig. 6 Experimental system

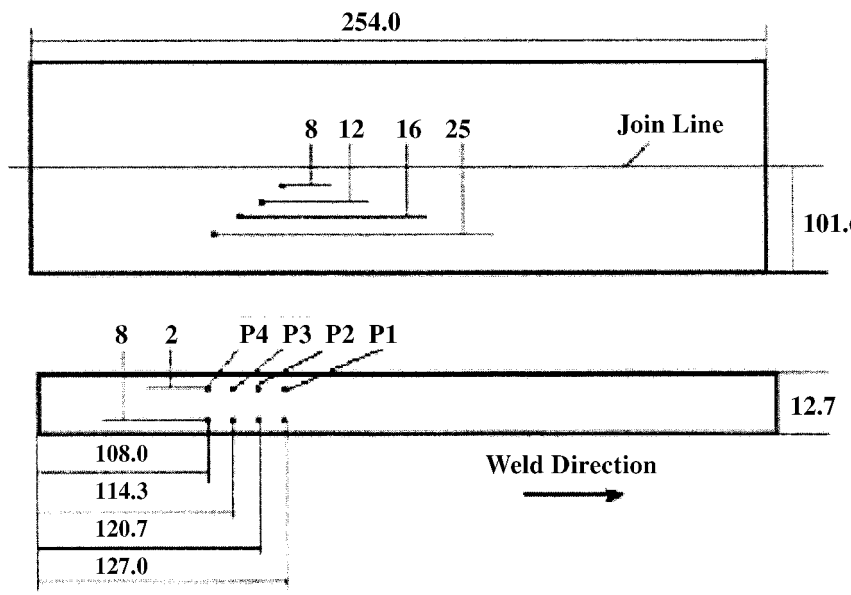

Fig. 7 Workpiece and thermocouples

A force transducer is used to measure the applied force during the weld. Eight type-K NiAl/NiCr thermocouples are embedded in the workpiece to measure the temperature history. The locations of measuring points 1, 2, 3 and 4 are 2.0 mm beneath the upper surface; points 1, 2, 3 and 4 are 8, 12, 16 and 25 mm from the joint line respectively. Therefore, points 1, 2 and 3 are within the tool shoulder distance and point 4 is just outside the shoulder outer edge. Points 5, 6, 7 and 8 are 4.3 mm from the bottom surface. The dimensions of the welding workpiece and the locations of the thermocouples are shown in Fig. 7.

Figure 8 shows the measured temperatures of the upper layer measuring points 1, 2, 3 and 4 at rotational speeds of 914, 637 and 344 r/min respectively. The weld speed is 1.59 mm/s. It can be found that the measured temperature peaks at points 1, 2 and 3 at all rotational speeds are close to the material melting point, 855 K. It

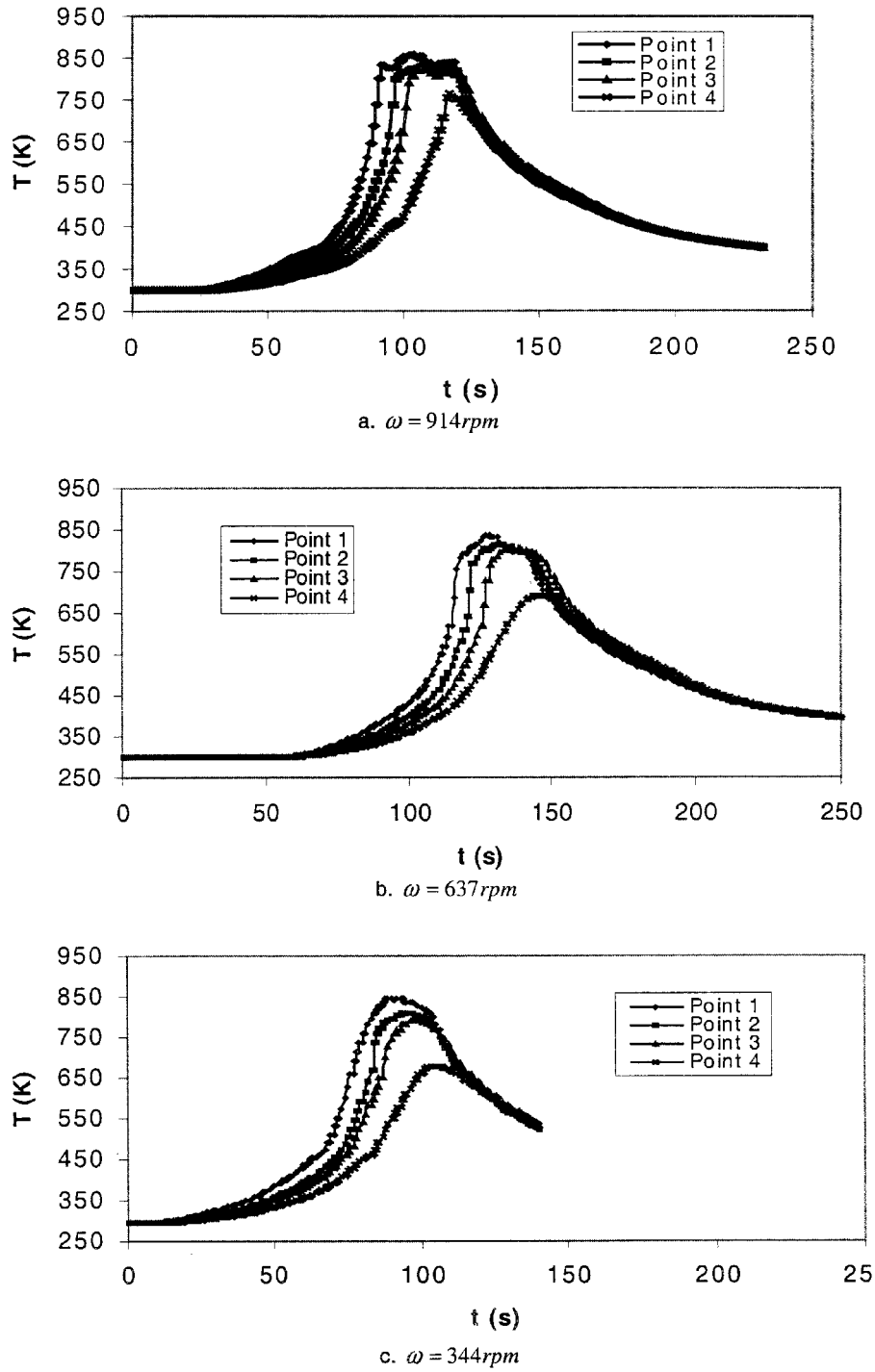

Fig. 8 Measured temperature at different rotational speeds (v = 1.59 mm/s)

should also be noted that these measuring points are 2.0 mm beneath the tool shoulder/workpiece interface. It is expected that the maximum temperature at the tool shoulder/workpiece interface could be even higher.

Another interesting phenomenon is noticed from the measured temperatures. At the welding speed of 1.59 mm/s, the measured temperatures stay nearly constant for a period of time in points 1, 2 and 3 at higher rotational speeds of 637 or 914 r/min. At the rotational speed of 914 r/min, the measured temperature at points 1, 2 and 3 remain unchanged for about 28, 26 and 22 s respectively. The time needed for the shoulder to pass over the corresponding measuring points can be approximated by $\Delta t = 2R_{sh}/v$. The corresponding passing-over times are 31, 29 and 27 s respectively. The duration time of the temperature constant in measuring points 1, 2 and 3 can coincide with the passing-over time of the shoulder. At these welding conditions, the temperatures of the points at the tool shoulder/workpiece interface are close to the material melting temperature.

The measured temperature at point 4, which is just outside the shoulder covering area, does not follow the

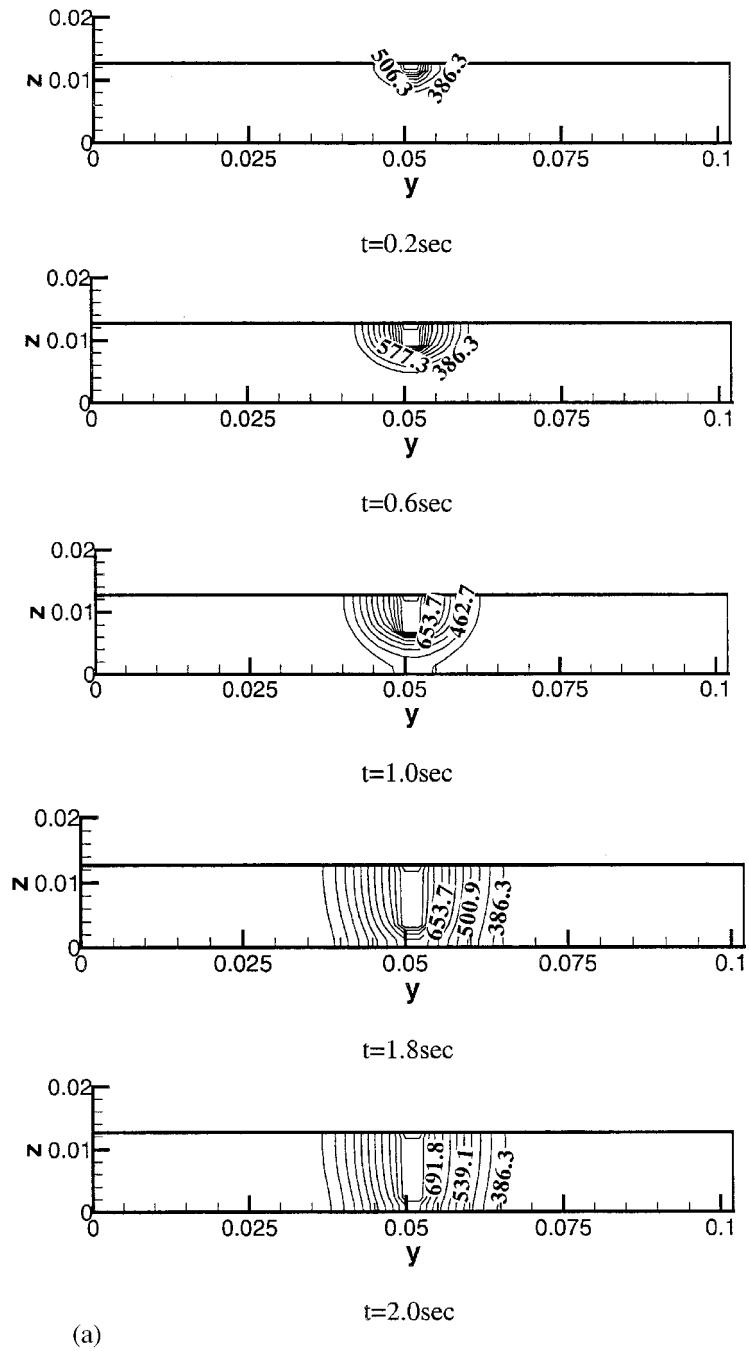

(a)

Fig. 9 (continued over)

above-noticed tendency. It can also be found that a significant increase in the rotational speed does not cause a significant increase in the measured peak temperature. The measured temperatures at points 1, 2 and 3 at a rotational speed of 914 r/min are close to the measured temperatures at the corresponding points at 637 r/min. In a homogeneous material undergoing FSW these results can be explained by the fact that the material flow stress drops rapidly near the material melting point, thus causing the heat generation rate in the workpiece to go to near zero, even though the tool rotational speed has increased. This helps to keep the FSW in a solid state.

5 NUMERICAL RESULTS

An $80 \times 50 \times 12$ grid is used in the calculation. The time marching step is 0.02 s. In order to investigate how the weld parameters affect the heat transfer process, different weld conditions are adopted in the calculation.

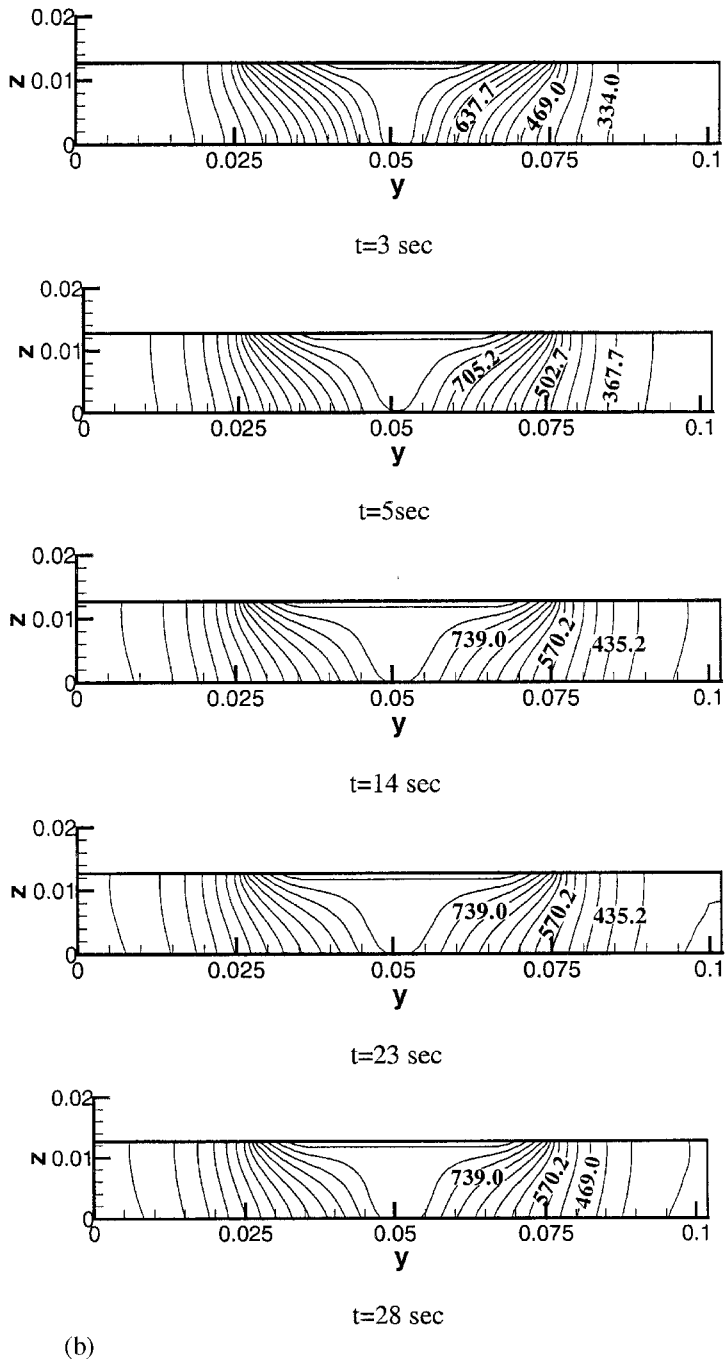

(b)

Fig. 9 (continued over)

5.1 Temperature field

5.1.1 The penetration period

During this period, the rotating tool pin slowly penetrates the workpiece. The pin penetrating speed is chosen to be 5 mm/s in the calculation; therefore, the total penetration time is about 12.7/5 = 2.54 s.

Figure 9a shows the calculated temperature contour at 0.2, 1.0 and 2.0 s respectively. Figure 9a clearly illustrates the heat transfer process in the workpiece during the pin penetration period. The temperature near the tool pin increases very fast while the pin plunges deeper into the workpiece, and the volumetric heat source region moves at the pin penetration speed.

5.1.2 The main welding period

This period is the main weld period of FSW. During this period, the tool traverses along the join line at the

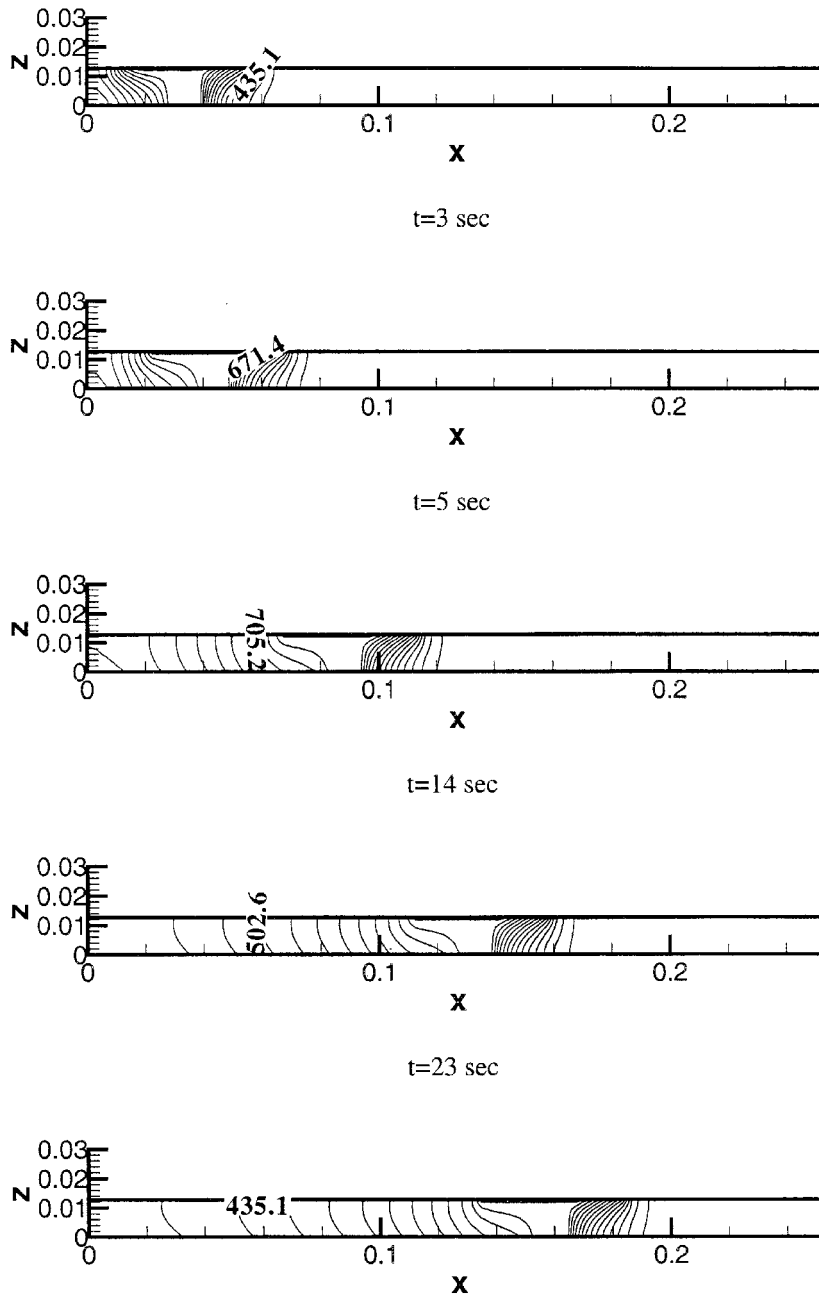

(c)

Fig. 9 (continued over)

welding speed. The welding speed is 5 mm/s. The duration time of this period is chosen to be 30 s in the calculation.

Figure 9b illustrates the calculated temperature distribution of the workpiece at 3.0, 14.0 and 28.0 s respectively. Figure 9b clearly illustrates the heat transfer process in the workpiece during the welding period. It is clear from the y–z cross-section view that the temperature pattern on the section perpendicular to the welding direction does not change much during the main welding period; therefore the heat transfer in this cross-section can be assumed to be quasi-steady during the main welding period. It is also found in the calculation that if the heat input is high, the calculated temperatures could be very close to the material melting temperature.

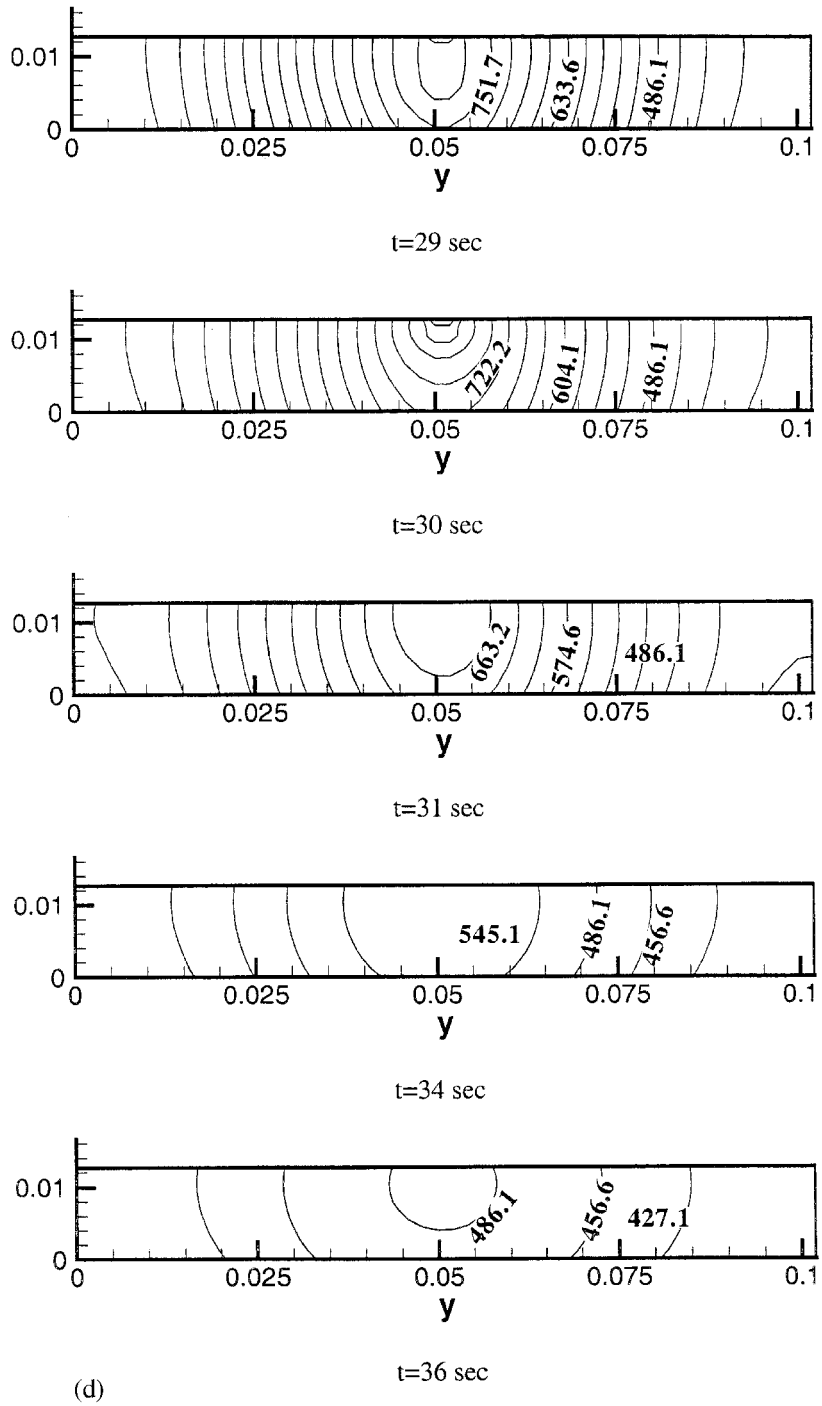

Fig. 9 Temperature contours during (a) the penetration period (front view), (b) the welding period (front view), (c) the welding period (side view) and (d) the pulling-out period (front view)

5.1.3 *The pulling-out period*

During this period, the heat flux generated by the tool shoulder is removed; the heat generated by the tool pin is slowly pulled out from the workpiece. The calculated temperature distributions at 32.0, 35.0 and 40.0 s during this period are shown in Fig. 9c. At the instant the pin is pulled out, the temperature of the workpiece is still high and then gradually drops down.

5.2 Microstructure analysis

The typical FSW microstructural morphology consists of the weld nugget, the thermal-mechanical-affected zone (TMAZ), the heat-affected zone (HAZ) and the base material. The microstructure morphology is believed to be related to the local thermal history. The shapes and grey levels on the microstructure morphology of the weld cross-section area are related to the local peak temperature experienced in each region.

Figure 10 shows the calculated isotherms of the peak temperatures in the welding zone compared to the experimentally obtained microstructure morphology. The tool rotational speed is 637 r/min and the welding speed is 1.59 mm/s. The calculated temperature field corresponds to the main welding period. It can be seen that the calculated peak temperature contours can accurately simulate the temperature history of the welding zone.

The value of the calculated peak temperature in the nugget is about 835 K, the calculated peak temperature of the TMAZ is in the range of 760–610 K and the calculated peak temperature in the HAZ is in the range of 610–480 K. The calculated temperatures in each weld zone coincide with the experimental measured results by Sato *et al.* for Al 6063 [**20**], which is similar to Al 6061 in chemical composition and physical properties.

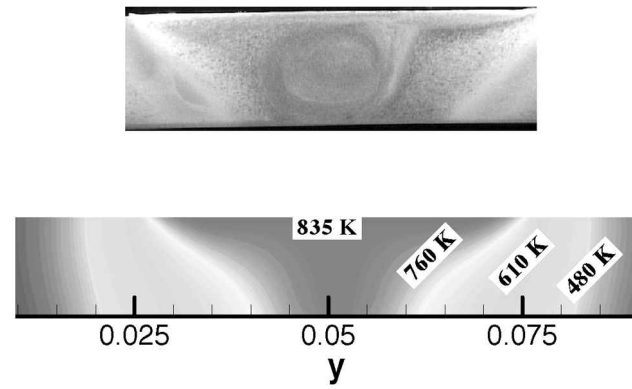

Fig. 10 Calculated isothermals versus microstructure morphology

5.3 Thermal history

The presented model can also be used to predict the thermal history at any position in the workpiece that can be used in predicting the weld zone hardness. Figure 11 shows the comparison of the calculated and measured temperature history in measuring point 2. The welding speed is 1.59 mm/s and the tool rotational speed is 637 r/min. The results show that the calculated curve

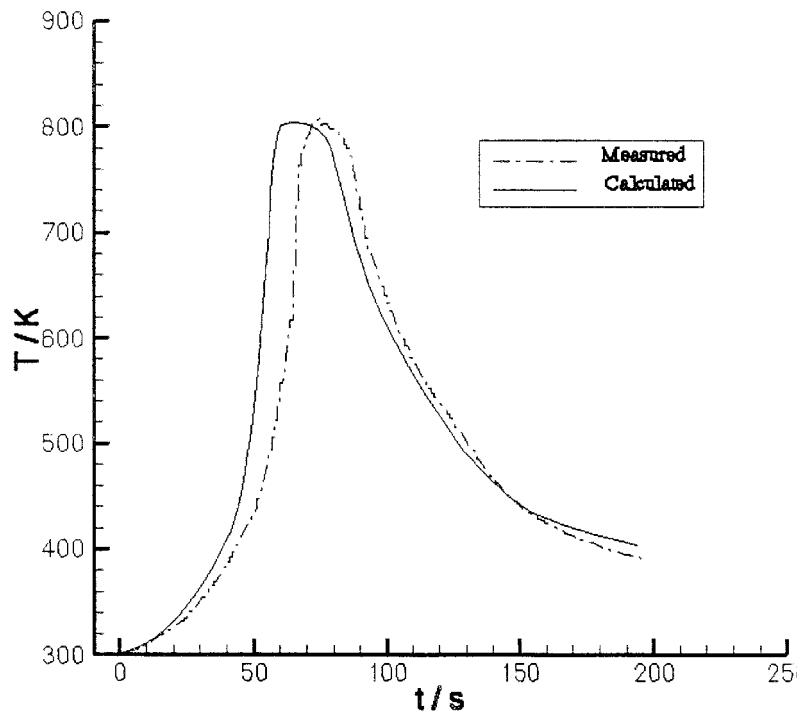

Fig. 11 Calculated and measured temperature history

and the measured curve are of the same shape and that the maximum temperatures on both curves are of the same value, which implies that the present model can accurately predict the heat transfer process in FSW.

6 CONCLUSIONS

A new heat transfer model used for modelling the heat generation and conduction in FSW is presented in this paper. The real temperature has also been measured in order to validate the modelled results. The following conclusions can be drawn:

1. This model can be applied in modelling the heat transfer process for friction stir welding.
2. The local temperatures immediately beneath the tool shoulder could be very close to the material melting temperature if the input heat flux is high enough.
3. The heat transfer in the section perpendicular to the welding direction can be assumed to be quasi-steady during the main welding period.
4. The plastic deformation heat can be modelled as a uniform volumetric heat generation.

ACKNOWLEDGEMENTS

The authors would like to express thanks to Dr J. Ouyang and Mr M. Valant for their valuable help during the experiments of part of this research. The work is financially supported by the US Department of Education, Grant P200A80806-98, and by the Texas High Education Coordinating Board, Grants 003613-022-1999 and 003613-0016-2001.

REFERENCES

1 **Thomas, M. W., Nicholas, J., Needham, J. C., Murch, M. G., Templesmith, P.** and **Dawes, C. J.** Friction stir butt welding. GB Pat. Application 9125978.8, December 1991; US Pat. 5460317, October 1995.

2 **Dawes, C. J.** An introduction to friction stir welding and its developments. *Weld. and Metal Fabrication*, January 1995, **63**(1), 13–16.

3 **Nicholas, E. D.,** *et al.* Friction stir welding—a decade on. In IIW Asian Pacific International Congress, Sydney, 29 October–2 November 2000.

4 **Chao, Y. J.** and **Qi, X.** Thermal and thermo-mechanical modeling of friction stir welding of aluminum alloy 6061-T6. *J. Mater. Processing and Mfg Sci.*, 1998, **7**, 215–233.

5 **Frigaard, Ø, Grong, Ø** and **Midling, O. T.** Modeling of the heat flow phenomena in friction stir welding of aluminum alloys. In Proceedings of the Seventh International Conference on *Joints in Aluminium* (*INALCO '98*), Cambridge, April 1998.

6 **Frigaard, Ø, Grong, Ø** and **Midling, O. T.** A process model for friction stir welding of age hardening aluminum alloys. *Metall. Mater. Trans. A*, May 2001, **32A**, 1189–1200.

7 **Gould, J. E.** and **Feng, Z.** (1998), Heat flow model for friction stir welding of aluminum alloys. *J. Mater. Processing and Mfg Sci.*, 1998, **7**, 185–194.

8 **Russell M. J.** and **Shercliff, H. R.** Analytical modeling of microstructure development in friction stir welding. In Proceedings of the 1st International Symposium on *Friction Stir Welding*, Thousand Oaks, California, June 1999.

9 **Colegrove, P.** 3 dimensional flow and thermal modeling of the friction stir welding process. In Proceedings of the 2nd International Symposium on *Friction Stir Welding*, Sweden, August 2000.

10 **Bendzsak, G. B., North, T. H.** and **Smith C. B.** An experimentally validated 3D model for friction stir welding. In Proceedings of the 2nd International Symposium on *Friction Stir Welding*, Sweden, June 2000.

11 **Smith, C. B., Bendzsak, G. B., North, T. H., Hinrichs, J. F., Noruk, J. S.** and **Heideman, R. J.** Heat and material flow modeling of the friction stir welding process. In Proceedings of Ninth International Conference on *Computer Technology in Welding* (Eds T. Siewert and C. Pollock), May 2000, 475–486.

12 **Dong, P., Lu, F., Hong, J. K.** and **Cao, Z.** Analysis of weld formation process in friction stir welding. In Proceedings of the 1st International Symposium on *Friction Stir Welding*, Thousand Oaks, California, June 1999.

13 **Askari, A. Silling, S., London, B.** and **Mahoney, M.** Modeling and analysis of friction stir welding process. In *Friction Stir Welding and Processing* (Eds K. Jata, M. Mahoney, R. S. Mishra, S. L. Semiatin and D. P. Field), 2001, pp. 43–54 (TMS Publisher).

14 **Fonda, R. W.** and **Lambrakos, S. G.** Analysis of friction stir welding using an inverse-problem approach. In *Friction Stir Welding and Processing* (Eds K. Jata, M. Mahoney, R. S. Mishra, S. L. Semiatin and D. P. Field), 2001, pp. 131–137 (TMS Publisher).

15 **Song, M.** and **Kovacevic, R.** A new heat transfer model for friction stir welding. *Trans. NAMRI/SME*, 2002, **30**, 565–572.

16 **Tang, W., Guo, X., McClure, J. C.** and **Murr, L. E.** Heat input and temperature distribution in friction stir welding. *J. Mater. Processing and Mfg Sci.*, 1998, **7**, 163–172.

17 **Mahoney, M. W., Rhodes, C. G., Flintoff, J. G., Spurling, R. A.** and **Bingel, W. H.** Properties of friction-stir-welded 7075 T651 aluminum. *Metall. Mater. Trans. A*, July 1998, **29A**, 1955–1964.

18 **Reynolds A. P.,** *et al.* Processing-property correlation in friction stir welds. *Mater. Sci. Forum*, 2000, **331–337**, 1719–1724.

19 **Kohn, G., Greenberg, Y., Makover, I.** and **Munitz, A.** Laser-assisted friction stir welding. *Weld. J.*, February 2002, 46–48.

20 **Sato, Y., Kokawa, H., Enomoto, M.** and **Jogan, S.** Microstructure evaluation of 6063 aluminum during friction stir welding. *Metall. Mater. Trans. A*, September 1999, **30A**, 2429–2437.

Copyright of Proceedings of the Institution of Mechanical Engineers -- Part B -- Engineering Manufacture is the property of Professional Engineering Publishing and its content may not be copied or emailed to multiple sites or posted to a listserv without the copyright holder's express written permission. However, users may print, download, or email articles for individual use.